Volume 8 | Number 12 | 21 June 2021

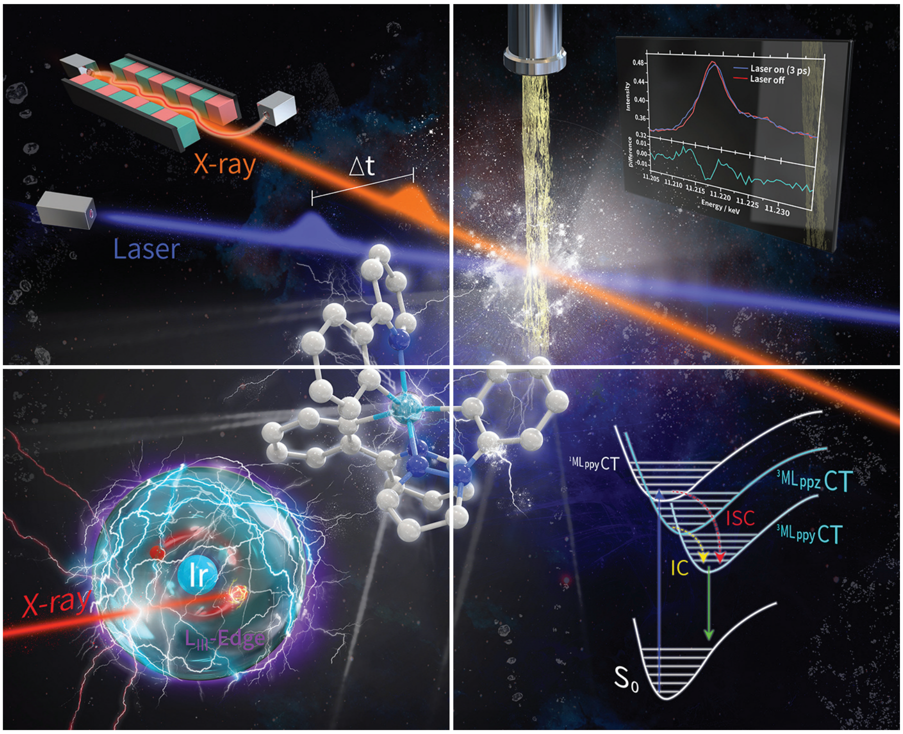

INORGANIC CHEMISTRY FRONTIERS

CCS 中国化学会 CHINESE CHEMICAL SOCIETY

PEKING UNIVERSITY 1898

ROYAL SOCIETY OF CHEMISTRY

rsc.li/frontiers-inorganic

INORGANIC CHEMISTRY
FRONTIERS

RESEARCH ARTICLE

View Article Online
View Journal | View Issue

Check for updates

Cite this: *Inorg. Chem. Front.*, 2021, **8**, 2987

Ultrafast excited state relaxation dynamics in a heteroleptic Ir(III) complex, *fac*-Ir(ppy)$_2$(ppz), revealed by femtosecond X-ray transient absorption spectroscopy†

Jungkweon Choi,[a,b] Mina Ahn,[c] Jae Hyuk Lee,[d] Doo-Sik Ahn,[a,b] Hosung Ki,[a,b] Inhwan Oh,[b] Chi Woo Ahn,[b] Eun Hyuk Choi,[b] Yunbeom Lee,[b] Seonggon Lee,[b] Jungmin Kim,[b] Dae Won Cho,[e] Kyung-Ryang Wee *[c] and Hyotcherl Ihee *[a,b]

Received 23rd December 2020,
Accepted 24th March 2021

DOI: 10.1039/d0qi01510e

rsc.li/frontiers-inorganic

A typical metal complex has a central metal surrounded by multiple ligands, which greatly affect the properties of the whole complex. Although heteroleptic complexes often exhibit substantially different behaviors from homoleptic complexes, systematic studies to explain their origins have been rare. Of special importance is to understand why the heteroleptic metal complex shows a more complicated excited state relaxation dynamics than the homoleptic metal complex. To address this issue, we investigated the excited state relaxation dynamics of a heteroleptic Ir(III) complex, *fac*-Ir(ppy)$_2$(ppz), and two homoleptic Ir(III) complexes, *fac*-Ir(ppy)$_3$ and *fac*-Ir(ppz)$_3$, using femtosecond X-ray transient absorption (fs-XTA) spectroscopy, ultrafast optical transient absorption (TA) spectroscopy, and DFT/TDDFT calculation. The data show that the ultrafast relaxation dynamics of ~450 fs, which is significantly faster than those of previous Ir(III) complexes with other ligands, is observed only in *fac*-Ir(ppy)$_2$(ppz) but not in the homoleptic Ir(III) complexes. Such dynamics observed for only heteroleptic Ir(III) complexes must originate from the heteroleptic character, and naturally, the inter-ligand energy transfer between two different types of ligands has been suggested to explain the fast dynamics. Both fs-XTA and TA data, however, favor the assignment of the ultrafast dynamics of ~450 fs to the internal conversion (IC) process from the ppz-localized ^{3}MLCT to the ppy-localized ^{3}MLCT. The DFT/TDDFT calculations support that the abnormally fast IC for *fac*-Ir(ppy)$_2$(ppz) is due to a large nonadiabatic coupling and the small energy gap between the two states.

Introduction

Ligands bound to the metal in a typical metal complex play critical roles in modulating the properties of the metal complex.[1–15] For example, the electronic states of ligands effectively modulate the photophysical properties, and depending on whether the ligands are of the same (homoleptic) or different (heteroleptic) kinds, the metal complexes exhibit different behaviors. Nevertheless, fundamental studies aimed at understanding the origins of the different properties of homoleptic and heteroleptic metal complexes have been sparsely reported. Cyclometalated Ir(III) complexes are one such example. They have initially been synthesized to be used as a light emitter in organic light-emitting diodes (OLEDs) and a photosensitizer in artificial photosynthesis[1,3–5,16–19] and have also attracted much attention as a promising photocatalyst due to their unique electronic state with heavy metal effect.[20–26] Their photophysical properties have been extensively investigated with various experimental and theoretical approaches.[3,4,16–19,26–36]

In the case of homoleptic Ir(III) complexes, the electronic excitation with visible light induces the formation of a singlet metal-to-ligand charge transfer (^{1}MLCT) state. Compared to other transition metal complexes with different central metals, Ir(III) complexes have the triplet metal-centered d–d states (^{3}MC) that have higher energies than their emissive states (so-called triplet metal-to-ligand charge transfer state, ^{3}MLCT). Thus, the excited molecules in the ^{1}MLCT state relax to the

---

[a] Center for Nanomaterials and Chemical Reactions, Institute for Basic Science, Daejeon 34141, Republic of Korea

[b] Department of Chemistry and KI for the BioCentury, Korea Advanced Institute of Science and Technology (KAIST), Daejeon 34141, Republic of Korea. E-mail: hyotcherl.ihee@kaist.ac.kr

[c] Department of Chemistry, Daegu University, Gyeongsan 38453, Republic of Korea. E-mail: krwee@daegu.ac.kr

[d] Pohang Accelerator Laboratory, Pohang, 37673, Republic of Korea

[e] Department of Advanced Materials Chemistry, Korea University, Sejong Campus, Sejong 30019, Korea

† Electronic supplementary information (ESI) available. See DOI: 10.1039/d0qi01510e

^{3}MLCT state through the ultrafast intersystem crossing (ISC) process within 100 fs due to the strong spin–orbit coupling (SOC) of the Ir atom.[30,32,37,38] It is known that the lowest triplet excited states of most Ir(III) complexes in solution are ^{3}MLCT states. Therefore, the majority of excited molecules transit to the ^{3}MLCT state and then return to the ground state *via* phosphorescence with a high phosphorescence quantum yield (Φ_P = 0.8–1). On the one hand, for Ir(III) complexes with extended π-conjugated ligands, their lowest triplet excited states are changed to the ligand-centered $^3\pi,\pi^*$ state (^{3}LC). Consequently, Ir(III) complexes with a largely expanded π-conjugation show the deactivation process from the ^{3}MLCT state to the ^{3}LC state,[39–41] resulting in the emission from the ^{3}LC state. In contrast to homoleptic Ir complexes, heteroleptic Ir(III) complexes exhibit more complicated photophysical dynamics due to the possibilities of inter-ligand interactions such as ligand-to-ligand charge transfer (LLCT)[18,26,31,42–44] and ligand-to-ligand energy transfer (LLET).[27,28,42,45,46] Tschierlei *et al.* reported the LLCT dynamics occurring with a time constant of 30 ps in $[Ir(ppy)_2(bpy)]^+$ and $[Ir(ppy)_2(bpy(COOH)_2)]^+$ of the type $[Ir(C\hat{}N)_2(N\hat{}N)]^+$.[26] Cho *et al.* demonstrated that the LLCTs for $[Ir(dfppy)_2(tpphz)]^+$ and $[Ir(dfppy)_2(dpq)]^+$ of the type $[Ir(C\hat{}N)_2(N\hat{}N)]^+$ take place with time constants of 17 and 5 ps, respectively, and proposed that the energy barrier between cyclometalating and ancillary ligands is responsible for the different time constants for LLCT dynamics of two Ir complexes.[31] You *et al.* reported LLETs for heteroleptic Ir(III) complexes of the type $Ir(C\hat{}N)_2(O\hat{}N)$ occurring with a time constant of *ca.* 6–7 ns.[27] In addition, the theoretical calculation for some heteroleptic Ir complexes showed that an ultrafast internal conversion (IC) process within triplet manifolds can occur as fast as the ISC from ^{1}MLCT to ^{3}MLCT.[19] However, despite numerous experimental and theoretical studies, the determining factors for the fast excited state relaxation dynamics for Ir(III) complexes, especially heteroleptic Ir(III) complexes, are still elusive.

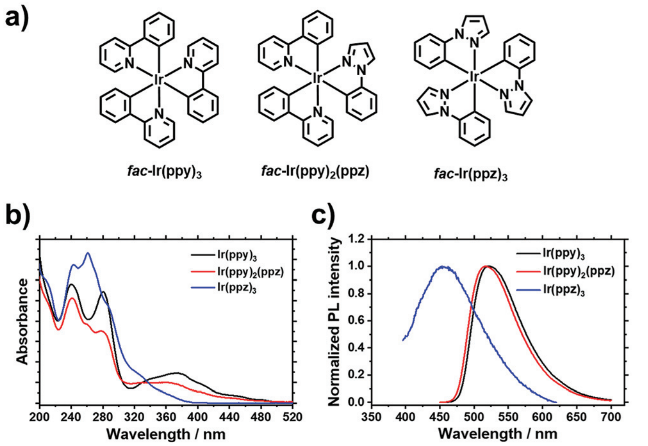

Fig. 1 (a) Structure of the homoleptic Ir(III) complexes (*fac*-Ir(ppy)$_3$ and *fac*-Ir(ppz)$_3$) and the heteroleptic Ir(III) complex (*fac*-Ir(ppy)$_2$(ppz)) studied in this work. (b and c) UV–visible absorption and emission spectra of three compounds in acetonitrile. For emission spectra, λ_{ex} = 400 nm for *fac*-Ir(ppy)$_3$ and *fac*-Ir(ppy)$_2$(ppz), and λ_{ex} = 322 nm for *fac*-Ir(ppz)$_3$. The sample solutions were purged with argon gas.

To address this issue, we investigated the fast excited state relaxation dynamics of a heteroleptic Ir(III) complex of the type $Ir(C\hat{}N)_2(C\hat{}N)'$, *fac*-Ir(ppy)$_2$(ppz), using femtosecond X-ray transient absorption (fs-XTA) spectroscopy and ultrafast optical transient absorption (TA) spectroscopy. For comparison, we also studied two homoleptic Ir(III) complexes of the type $Ir(C\hat{}N)_3$, *fac*-Ir(ppy)$_3$ and *fac*-Ir(ppz)$_3$. The *fac*-Ir(ppy)$_2$(ppz) molecule contains two ppy (2-phenylpyridine) as cyclometalating ligands and one ppz (phenylpyrazole) as an ancillary ligand (Fig. 1a). Recent years have witnessed great advances in time-resolved structural probes such as time-resolved electron diffraction,[47–51] time-resolved X-ray liquidography (TRXL),[52–60] and time-resolved X-ray spectroscopy.[9,61–68] Among these, fs-XTA is an effective tool for studying the local conformation and electronic structure of core elements in the excited state,[9,61–65] and TA is a useful tool to investigate the change of the electronic state of a target molecule.[31,44–46,69,70] Many studies on transition metal complexes using fs-XTA have provided information for the change in the metal–ligand bond length and MLCT dynamics occurring after the excitation with visible light.[9,62,71–75] Our fs-XTA and TA data show that the heteroleptic Ir(III) complex, *fac*-Ir(ppy)$_2$(ppz), has the ultrafast relaxation dynamics of ~450 fs, which is faster than those observed in previous Ir(III) complexes with different ligands, and is not observed in the counterpart homoleptic Ir(III) complexes (*fac*-Ir(ppy)$_3$ and *fac*-Ir(ppz)$_3$) (see Fig. S7†). We propose that this unique ultrafast dynamics observed only for the heteroleptic Ir(III) complex corresponds to the internal conversion (IC) process from the ppz-localized ^{3}MLCT state (denoted as $^3ML_{ppz}CT$) to the ppy-localized ^{3}MLCT state (denoted as $^3ML_{ppy}CT$) and is probably due to the large nonadiabatic coupling as well as the small energy gap between the two states.

In addition, the TDDFT calculations demonstrate that the formation of the $^3ML_{ppy}CT$ state, which is the lowest triplet MLCT state, induces the conformational change in *fac*-Ir(ppy)$_2$(ppz). We thoroughly discuss the excited state relaxation dynamics of *fac*-Ir(ppy)$_2$(ppz) occurring after the photoexcitation.

Results and discussion

Relative energy levels from UV–visible absorption spectra

The UV–visible absorption spectra of free ppy and ppz ligands exhibit the absorption band corresponding to the π–π* transition at ~275 nm and ~255 nm, respectively (Fig. S8†). The shorter wavelength for the ppz ligand indicates that the singlet ligand centered (^{1}LC) state of the ppz ligand has higher energy than that of the ppy ligand. All three Ir complexes show intense absorption bands corresponding to π–π* transitions of ligands at a short wavelength (<300 nm) and the broad absorption bands attributed to ^{1}MLCT/^{3}MLCT states at a long wavelength (≥320 nm) (Fig. 1b). The absorption spectrum of *fac*-

Ir(ppy)$_2$(ppz) is about the average of those of *fac*-Ir(ppy)$_3$ and *fac*-Ir(ppz)$_3$. Wang *et al.*[76] and Hofbeck *et al.*[77] assigned the intense absorption band at ~385 nm of *fac*-Ir(ppy)$_3$ to the ^{1}ML$_{ppy}$CT transition and the weak broad shoulder band in the longer wavelength range (450–510 nm) to the ^{3}ML$_{ppy}$CT transition and its vibrational satellites. Based on their assignments, we attribute the absorption band of *fac*-Ir(ppy)$_2$(ppz) observed over 360 nm to ^{1}ML$_{ppy}$CT/^{3}ML$_{ppy}$CT states. In contrast, *fac*-Ir(ppz)$_3$ exhibits the absorption band due to the transition to ^{1}ML$_{ppz}$CT at a short wavelength (320–360 nm) and the transition to ^{3}ML$_{ppz}$CT over 400 nm (see Fig. 1b). For the ^{3}ML$_{ppz}$CT ← S$_0$ transition of *fac*-Ir(ppz)$_3$, a feeble absorption band at ~410 nm is clearly observed in the high concentration solution (Fig. S9†). Based on the absorption wavelengths of MLCT states observed from three Ir complexes, we estimate that the spin-allowed ppz-localized MLCT states (^{1}ML$_{ppz}$CT) of *fac*-Ir(ppz)$_3$ have higher energy than the spin-allowed ppy-localized MLCT states (^{1}ML$_{ppy}$CT) of *fac*-Ir(ppy)$_3$ and *fac*-Ir(ppy)$_2$(ppz). In addition, the spectroscopic results demonstrate that in *fac*-Ir(ppy)$_2$(ppz) the energy level of ^{3}ML$_{ppz}$CT is higher than that of ^{3}ML$_{ppy}$CT but is lower than that of ^{1}ML$_{ppy}$CT. The relatively closely spaced absorption bands of 410 and 450–510 nm corresponding to the ^{3}ML$_{ppz}$CT ← S$_0$ transition of *fac*-Ir(ppz)$_3$ and the ^{3}ML$_{ppy}$CT ← S$_0$ transition of *fac*-Ir(ppy)$_3$, respectively, indicate that the energy gap between ^{3}ML$_{ppz}$CT and ^{3}ML$_{ppy}$CT is quite small.

Emission spectra

To confirm the relative energy levels of ^{3}ML$_{ppz}$CT and ^{3}ML$_{ppy}$CT states, we measured the emission spectra of *fac*-Ir(ppz)$_3$, *fac*-Ir(ppy)$_3$ and *fac*-Ir(ppy)$_2$(ppz) in acetonitrile. Generally, the lowest emissive state of an Ir(III) complex is the ^{3}MLCT state formed through the fast ISC process. As shown in Fig. 1c, *fac*-Ir(ppy)$_3$ and *fac*-Ir(ppy)$_2$(ppz) have strong emission bands at ~520 and ~515 nm, respectively, whereas *fac*-Ir(ppz)$_3$ exhibits a feeble emission band at ~455 nm. The emission intensities of all three Ir complexes are significantly quenched by the presence of oxygen, indicating that the observed emissions are phosphorescence from the spin-forbidden ^{3}MLCT state (see Fig. S10†). In argon-saturated acetonitrile, the Φ_P values of *fac*-Ir(ppy)$_3$ and *fac*-Ir(ppy)$_2$(ppz) were found to be 0.97 and 0.98, respectively. The corresponding Φ_P value of *fac*-Ir(ppz)$_3$ was reported to be 0.002.[33] These high Φ_P values for *fac*-Ir(ppy)$_3$ and *fac*-Ir(ppy)$_2$(ppz) indicate the absence of non-radiative processes to induce phosphorescence quenching for these molecules. The weak phosphorescence of *fac*-Ir(ppz)$_3$ at room temperature is probably due to the opening of a non-radiative and/or nonreactive decay process from the lowest ^{3}MLCT state to the higher-lying metal-centered state (^{3}MC) as proposed by Pomarico *et al.*[32] It is noteworthy that the phosphorescence spectrum of *fac*-Ir(ppy)$_2$(ppz) resembles that of *fac*-Ir(ppy)$_3$. This similarity suggests that the low-lying triplet emissive states of both *fac*-Ir(ppy)$_3$ and *fac*-Ir(ppy)$_2$(ppz) are of the same origin. Previous studies for *fac*-Ir(ppy)$_3$ and *fac*-Ir(ppz)$_3$ demonstrated that the emissive states of *fac*-Ir(ppy)$_3$ [76,77] and *fac*-Ir(ppz)$_3$ [32,33] are the ^{3}ML$_{ppy}$CT and ^{3}ML$_{ppz}$CT states, respectively. These results suggest that the lowest-lying triplet emissive state of *fac*-Ir(ppy)$_2$(ppz) is the ^{3}ML$_{ppy}$CT state. To confirm the emissive state of *fac*-Ir(ppy)$_2$(ppz), we measured the phosphorescence spectra and lifetimes of *fac*-Ir(ppz)$_3$ and *fac*-Ir(ppy)$_2$(ppz) in 2-methyltetrahydrofuran at 77 K. As shown in Fig. S11,† at 77 K, *fac*-Ir(ppz)$_3$ shows an emission spectrum with a vibronic structure at around 414 nm. The emission lifetime is determined to be 15 μs. Our emission spectrum and lifetime of *fac*-Ir(ppz)$_3$ are also consistent with those reported in a previous study.[33] Compared to *fac*-Ir(ppz)$_3$, *fac*-Ir(ppy)$_2$(ppz) exhibits a largely red-shifted emission with a vibronic structure at ~489 nm. The emission lifetime is determined to be 4.4 μs. These differences in the phosphorescence spectra and lifetimes indicate that the emission observed from *fac*-Ir(ppy)$_2$(ppz) does not come from the ^{3}ML$_{ppz}$CT state. Here, it is noteworthy that the phosphorescence spectra of *fac*-Ir(ppy)$_2$(ppz) at 77 K and room temperature show peaks at similar wavelengths. This supports that the emission observed from *fac*-Ir(ppy)$_2$(ppz) at 77 K is phosphorescence from the ^{3}ML$_{ppy}$CT state, whose energy level is lower than that of ^{3}ML$_{ppz}$CT.

Femtosecond X-ray transient absorption spectroscopy

To investigate if *fac*-Ir(ppy)$_2$(ppz) has any ultrafast excited state relaxation dynamics such as MLCT, LLCT, LLET, IC and ISC, we measured the fs-XTA spectrum for the Ir L$_{III}$-edge in acetonitrile. Fig. 2a compares the static and transient Ir L$_{III}$-edge spectra of *fac*-Ir(ppy)$_2$(ppz) measured in the range from 11.200 keV to 11.235 keV. In the ground state, the t$_{2g}$ orbital of the Ir atom in the Ir complex is occupied with six electrons. Upon excitation at 400 nm, the electron density from the metal valence orbitals is transferred to the π* orbitals of ligands, resulting in the formation of the MLCT state. Consequently, the t$_{2g}$ orbitals in ^{1}MLCT and ^{3}MLCT states are occupied with five electrons, yielding one vacancy. This vacancy in the d orbital may lead to the appearance of a pre-edge feature and a blue shift of the edge band. As shown in Fig. 2a, the ground state absorption spectrum of *fac*-Ir(ppy)$_2$(ppz) shows two main bands at around 11.218 and 11.227 keV corresponding to 2p$_{3/2}$ → 5d (e$_g$) and shake-up transitions, respectively. It is known that the shake-up transition consists of two electron transitions: t$_{2g}$ → π* and the tail of 2p$_{3/2}$ → 5d (e$_g$).[71–73] On the one hand, the transient absorption spectrum (Fig. 2a) exhibits a new absorption band at 11.213 keV and the blue-shifted absorption corresponding to the 2p$_{3/2}$ → 5d (e$_g$) transition, and consequently, the transient difference spectra show an up–down–up feature (Fig. 2c). This feature is consistent with those for Ir(ppy)$_3$ and Ir(ppz)$_3$,[71,73] supporting that the photo-induced MLCT efficiently occurs in *fac*-Ir(ppy)$_2$(ppz). Based on the previous studies for metal complexes using X-ray transient absorption spectroscopy, we attribute the absorption around 11.213 keV to 2p$_{3/2}$ → 5d (t$_{2g}$) transition. To quantify the kinetics of *fac*-Ir(ppy)$_2$(ppz) in acetonitrile, we analyzed the time profiles monitored at 11.213, 11.218 and 11.221 keV. All three time profiles were fitted by bi-exponential functions with shared relaxation times of 420 ± 140 fs and >1 ns (Fig. 2b). The

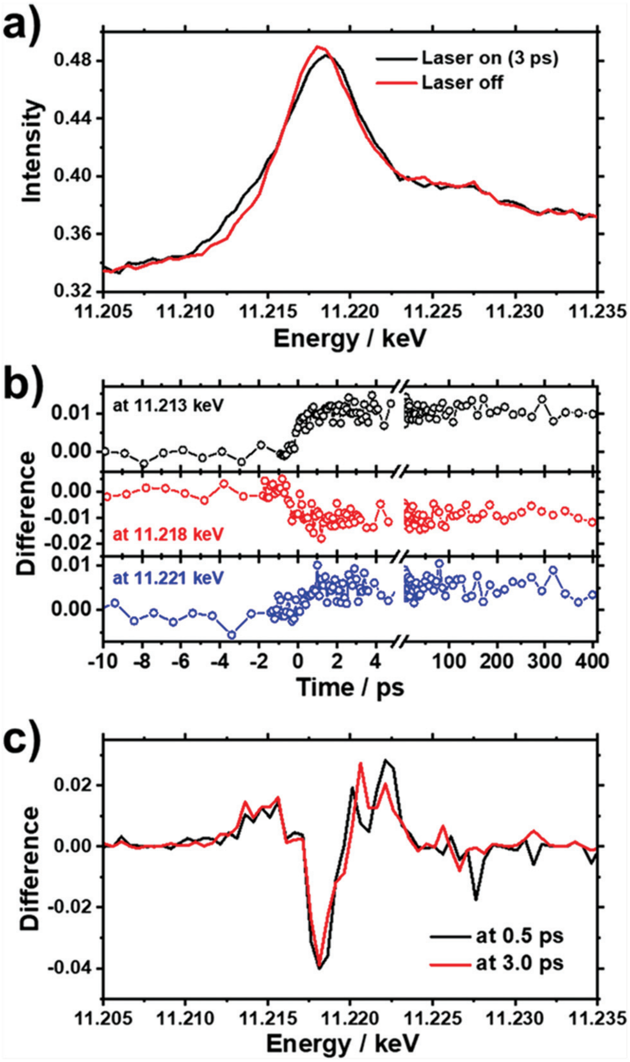

Fig. 2 (a) Time-resolved X-ray absorption spectra of *fac*-Ir(ppy)$_2$(ppz) in acetonitrile (λ_{ex} = 400 nm). (b) Time profiles monitored at 11.213, 11.218 and 11.221 keV. (c) Calibrated transient difference spectra measured at 0.5 and 3.0 ps. The calibrated difference curves were obtained using the XTA spectrum of the reference sample, *fac*-Ir(ppy)$_2$(bpy) (see the ESI†).

last relaxation time (>1 ns) could not be precisely determined due to the limited time range of our experiments and is essentially a constant. Here, one possibility that may explain 420 fs and therefore has to be considered is the nonradiative process from the ^{3}MLCT state to the ^{3}MC state, which induces phosphorescence quenching. Such a nonradiative decay through the ^{3}MC state generated with Ir–N bond rupture was suggested by Sajoto *et al.* to explain the low Φ_P value of *fac*-Ir(ppz)$_3$.[33] Pomarico *et al.* proposed that the weak emission of *fac*-Ir(ppz)$_3$ is probably due to the nonradiative decay process from the higher-lying MC state to the ground state.[32] However, as noted above, the high Φ_P value (0.98) of *fac*-Ir(ppy)$_2$(ppz) implies that the ^{3}MLCT → ^{3}MC transition does not occur. Using XTA, Cordones *et al.* also reported that in [Ru(bpy)$_2$(pyESO)]$^{2+}$, the formation of the hexa-coordinated ^{3}MC state induces a significant change in the transient difference spectrum.[9] By contrast, in the case of *fac*-Ir(ppy)$_2$(ppz), the transient difference spectra measured at different delay times are nearly identical to each other (Fig. 2c). To confirm our interpretation that the ^{3}MLCT → ^{3}MC transition in *fac*-Ir(ppy)$_2$(ppz) does not occur, we calculated the transient difference curves for ^{3}MLCT and ^{3}MC states of *fac*-Ir(ppy)$_2$(ppz) and compared them with the experimental difference curves measured at 0.5 and 3 ps. To start with, we calculated the minimum energy structure of *fac*-Ir(ppy)$_2$(ppz) in the triplet excited state using TDDFT. In the triplet excited state, *fac*-Ir(ppy)$_2$(ppz) has two optimized structures, T1$_{MLCT}$ and T2$_{MC}$, with MLCT and MC characters, respectively (see Fig. 3a). As shown in Fig. 3b, the calculated difference curve using the structure of T1$_{MLCT}$ is significantly different from that using the structure of T2$_{MC}$. The simulated difference curve for T1$_{MLCT}$ shows two positive peaks at 11.215 and 11.221 keV and one negative peak at 11.218 keV, whereas the simulated difference curve for T2$_{MC}$ exhibits positive and negative peaks at 11.216 and 11.220 keV, respectively (Fig. 3b). The simulated difference curve using the structure of T1$_{MLCT}$ is consistent with the experimental curves measured at 0.5 and 3 ps (Fig. 3c), whereas the simulated difference curve for T2$_{MC}$ is not. In addition, the energy level (2.80 eV) of the ^{3}MLCT state is lower than that (3.03 eV) of the ^{3}MC state. These calculation results confirm that the ^{3}MLCT → ^{3}MC transition is less plausible. Therefore, we ruled out the scenario that 420 fs is due to the formation of the ^{3}MC state, and thus the last relaxation time (>1 ns) should be attributed to the lifetime of the long-lived ^{3}MLCT state. As explained above, the lowest-lying ^{3}MLCT state of *fac*-Ir(ppy)$_2$(ppz) is the ^{3}ML$_{ppy}$CT state. Considering the rising feature observed in time profiles (Fig. 2b), the dynamics of 420 fs should correspond to the relaxation dynamics to form the ^{3}ML$_{ppy}$CT state. One plausible candidate relaxation dynamics responsible for the formation of the ^{3}ML$_{ppy}$CT state is ISC from ^{1}ML$_{ppy}$CT. On the other hand, since *fac*-Ir(ppy)$_2$(ppz) has two different ligands, ppy and ppz, its ^{3}MLCT is the mixed state of ^{3}ML$_{ppz}$CT and ^{3}ML$_{ppy}$CT. As mentioned above, the steady-state spectroscopic results demonstrate that the energy level of ^{3}ML$_{ppz}$CT is lower than that of ^{1}ML$_{ppy}$CT but is higher than that of ^{3}ML$_{ppy}$CT. In this regard, the IC from ^{3}ML$_{ppz}$CT to ^{3}ML$_{ppy}$CT is another plausible candidate. Similarly, Pomarico *et al.* reported that in the case of Ir(ppy)$_2$(bpy), the relaxation from a ppy-centered MLCT state to a bpy-centered MLCT state takes place with *ca.* 1.5 ps time constant, which includes some vibrational relaxation.[32] Thus, two candidates for the formation of ^{3}ML$_{ppy}$CT need to be considered: (i) ISC from ^{1}ML$_{ppy}$CT to ^{3}ML$_{ppy}$CT and (ii) IC from ^{3}ML$_{ppz}$CT to ^{3}ML$_{ppy}$CT.

Optical transient absorption spectroscopy

Numerous experimental and theoretical studies for homoleptic and heteroleptic Ir complexes have suggested that the ^{1}MLCT state generated by excitation with visible light relaxes to ^{3}MLCT *via* ISC within 100 fs.[30,32,37,38] Although the previously reported ISC processes are much faster than 420 fs

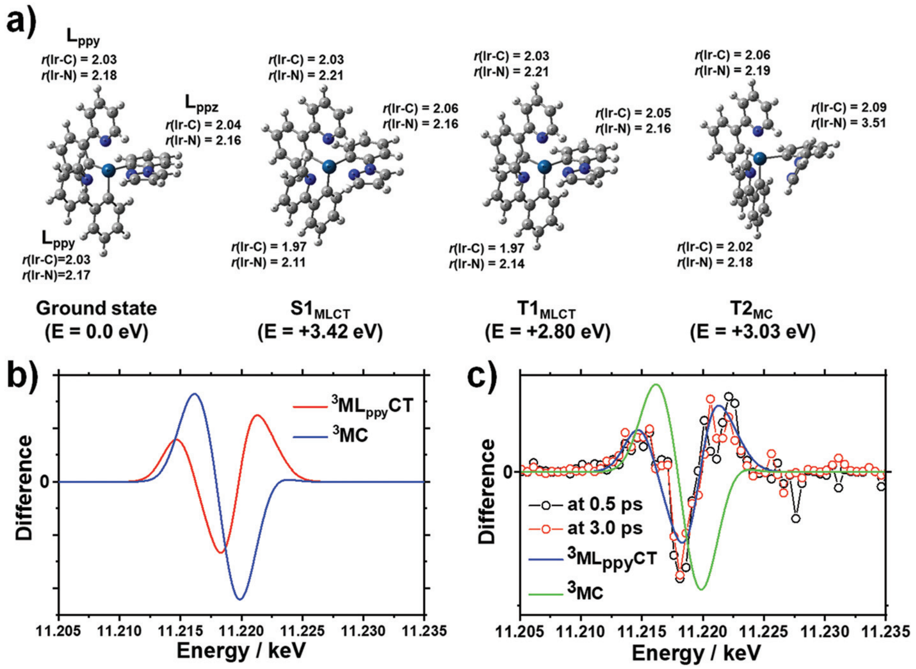

Fig. 3 (a) DFT-calculated structures and relative energies for S_0, S_1, and T_1 states. r(Ir–C) or r(Ir–N) indicates the bond lengths between Ir and adjacent carbon or nitrogen atoms (unit: angstrom). (b) Simulated difference curves for $T1_{MLCT}$ and $T2_{MC}$. (c) Comparison of the experimental transient difference spectra and the simulated difference curves for $T1_{MLCT}$ and $T2_{MC}$.

observed for *fac*-Ir(ppy)$_2$(ppz) in this study, one cannot rule out the possibility that 420 fs is due to ISC from ^{1}MLCT to ^{3}MLCT. Generally, the ISC can induce changes in the TA spectra, such as changes in the signal intensity and shape because of the energy gap between the singlet excited state and the triplet excited state. Indeed, the time-resolved TA technique has been frequently used to measure the triple–triplet absorption spectra of various organic and inorganic compounds.[26,30,31,44–46,78,79] To check this possibility and further assist the assignment of 420 fs, we measured the femtosecond optical TA spectra of *fac*-Ir(ppz)$_3$ and *fac*-Ir(ppy)$_2$(ppz) in acetonitrile. As shown in Fig. S12,† the TA spectra of *fac*-Ir(ppz)$_3$ exhibit a strong excited state absorption (ESA) band at around 480 nm and a weak ESA band over 550 nm. The time profiles of *fac*-Ir(ppz)$_3$ recorded at 490 and 580 nm show a very long-lived component (>1 ns), whose intensity is essentially constant. This long-lived component should stem from the long lifetime of ^{3}ML$_{ppz}$CT formed by the fast ISC (<100 fs). The absence of the fast component corresponding to ISC indicates that the ^{3}MLCT state of *fac*-Ir(ppz)$_3$ is rapidly formed through ISC and vibrational relaxation within 100 fs. The TA spectra for *fac*-Ir(ppy)$_2$(ppz) exhibit a strong ESA band at around 515 nm and a weak ESA band over 600 nm, as shown in Fig. 4a. The time profiles of the TA recorded at 515 and 670 nm exhibit a fast rise component of hundreds of femtoseconds, which is absent in the time profile for *fac*-Ir(ppz)$_3$, in addition to the very long-lived component (>1 ns). These time profiles of *fac*-Ir(ppy)$_2$(ppz) can be satisfactorily fitted by a bi-exponential function with two relaxation times of 470 ± 68 fs and >1 ns (Fig. 4b). The

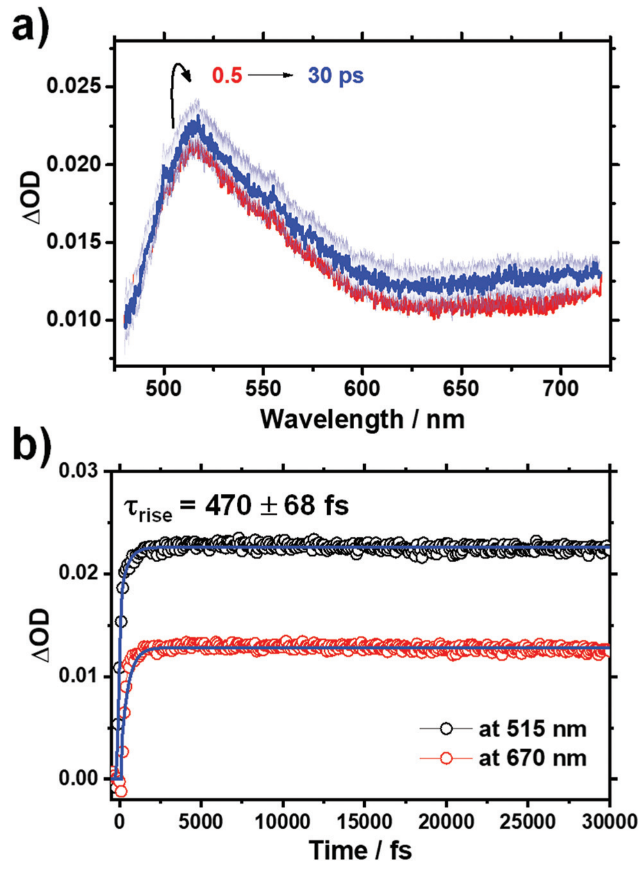

Fig. 4 (a) Transient absorption spectra of *fac*-Ir(ppy)$_2$(ppz) in acetonitrile (λ_{ex} = 400 nm). (b) Time profiles monitored at 515 and 670 nm.

time constant of 470 fs is essentially the same as that determined by fs-XTA (420 fs), considering the experimental errors. This consistency implies that the same ultrafast relaxation dynamics is observed by two different techniques. As shown in Fig. 4a, the spectral change due to the fast relaxation process is not observed, although the signal intensity slightly increases. This result suggests that the fast relaxation dynamics observed here cannot be attributed to the first scenario (ISC from ^{1}MLCT to ^{3}ML$_{ppy}$CT). In this regard, we speculate that the ISC from ^{1}ML$_{ppy}$CT to ^{3}MLCT for *fac*-Ir(ppy)$_2$(ppz) occurs within 100 fs due to the Ir-induced strong SOC and the time constant of ~450 fs observed from both fs-XTA and TA experiments is due to the second scenario (IC from the ^{3}ML$_{ppz}$CT state to the ^{3}ML$_{ppy}$CT state). In this regard, many studies for Ir complexes have reported the spin-forbidden ^{3}MLCT transition due to the Ir-induced strong SOC. Considering the energy levels of the ^{3}ML$_{ppz}$CT state, the excitation at 400 nm can induce the ^{3}ML$_{ppz}$CT ← S_0 transition as well as the ^{1}ML$_{ppy}$CT ← S_0 transition.

Therefore, we conclude that the fast dynamics of ~450 fs observed from both XTA and TA experiments corresponds to the IC process from ^{3}ML$_{ppz}$CT to ^{3}ML$_{ppy}$CT. The fast IC process from ^{3}ML$_{ppz}$CT to ^{3}ML$_{ppy}$CT for *fac*-Ir(ppy)$_2$(ppz) is probably due to the large nonadiabatic coupling between ^{3}ML$_{ppz}$CT and ^{3}ML$_{ppy}$CT. Indeed, the steady-state spectroscopic results, which show a small energy gap between ^{3}ML$_{ppz}$CT and ^{3}ML$_{ppy}$CT, suggest the presence of a large nonadiabatic coupling between ^{3}ML$_{ppz}$CT and ^{3}ML$_{ppy}$CT.

DFT and TDDFT calculations

To verify this possibility for the large nonadiabatic coupling between ^{3}ML$_{ppz}$CT and ^{3}ML$_{ppy}$CT, we conducted the DFT and TDDFT calculations for *fac*-Ir(ppy)$_2$(ppz). The calculation results are presented in Fig. 3a and 5. As shown in Fig. 3a, the optimized geometry of *fac*-Ir(ppy)$_2$(ppz) in the ground state (S_0) has similar bond lengths between the Ir metal center and three ligands (r(Ir–C) = 2.03 Å and r(Ir–N) = 2.17 Å), meaning that three ligands symmetrically bind to the Ir atom. In contrast, the optimized geometries in the singlet and triplet excited states (S1$_{MLCT}$ and T1$_{MLCT}$) show that two ppy ligands asymmetrically bind to the Ir atom with different Ir–C or Ir–N bond lengths, while the Ir–C or Ir–N bond lengths associated with the ppz ligand are barely changed compared with that in the S_0 state (Fig. 3a). This result implies that the transition to the ^{3}MLCT state induces symmetry breaking in two bound ppy ligands of *fac*-Ir(ppy)$_2$(ppz). We calculated vertical transition energies in the singlet and triplet states (Fig. S13†) and simulated the absorption spectrum optimized in the ground state (Fig. 5). For comparison, we simulated the absorption spectra of *fac*-Ir(ppy)$_3$ and *fac*-Ir(ppz)$_3$ as well. As shown in Fig. 5, the simulated spectra for *fac*-Ir(ppy)$_3$, *fac*-Ir(ppz)$_3$, and *fac*-Ir(ppy)$_2$(ppz) reproduce their experimental absorption spectra well except that the absolute absorption maxima are overestimated. The calculation results demonstrate that the steady-state absorption band of *fac*-Ir(ppy)$_2$(ppz) at around 380 nm (Fig. 1b) is mainly due to the ^{1}ML$_{ppy}$CT transition mixed with the ^{1}L$_{ppz}$L$_{ppy}$CT transition character and the ^{1}ML$_{ppz}$CT state with a relatively weak oscillator strength has higher energy than ^{1}ML$_{ppy}$CT. These results are consistent with the steady-state spectroscopic results. Moreover, the TDDFT calculation (Fig. S13†) reveals that the three lowest triplet state energy levels are close to the lowest singlet excited energy level at the Franck–Condon geometry and the optimized geometry of the S_1 state and the energy difference between the lowest singlet and triplet state energy levels becomes larger at the T_1 state geometry. This result implies that the nearly degenerate singlet and triplet states at the Franck–Condon region might promote the strong SOC, leading to the efficient ISC, and the lowest triplet state is further stabilized by the geometrical rearrangement of ppy ligands, which prevents back-transition to the singlet state. The efficient ISC is consistent with the expected ultrafast ISC concluded based on the fs-XTA and TA data.

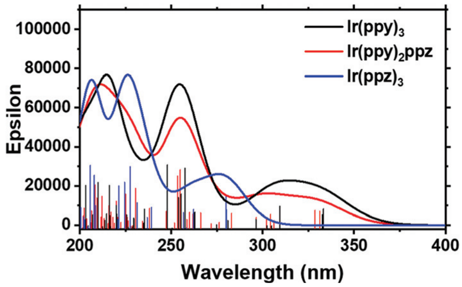

Fig. 5 TDDFT-calculated vertical excitation energies and simulated UV spectra of *fac*-Ir(ppy)$_2$ppz, *fac*-Ir(ppy)$_3$, and *fac*-Ir(ppz)$_3$ are represented with vertically dropped lines and line curves, respectively. For the simulated spectra, the bandwidth of 0.2 eV (FWHM) was applied to all peaks.

Inter-ligand interaction

Several studies for heteroleptic Ir(III) complexes have reported inter-ligand interactions such as LLCT and LLET occurring within a few and tens of picosecond time scales.[26,31,32,44–46] In this regard, the inter-ligand interaction is an alternative candidate against the IC process from ^{3}ML$_{ppz}$CT to ^{3}ML$_{ppy}$CT suggested in our study. It is worth noting, however, that XTA is not sensitive to an inter-ligand interaction occurring far from a given core element, although XTA data provide the information about the electronic structure of a given core element, such as type of bonding to neighbors, occupancy of valence orbitals and oxidation state. The LLET, which occurs through non-radiative dipole–dipole coupling between inter-ligands, does not induce a change in the electronic structure and oxidation state of a metal ion. Consequently, the inter-ligand interaction is not expected to induce any change in the fs-XTA spectrum at the Ir L$_{III}$-edge. Therefore, we suggest that the fast dynamics of ~450 fs observed from fs-XTA and TA experiments is due to the IC process from ^{3}ML$_{ppz}$CT to ^{3}ML$_{ppy}$CT rather than the inter-ligand interaction such as LLCT and LLET.

Reaction scheme for *fac*-Ir(ppy)$_2$(ppz)

To further elucidate the reaction scheme for *fac*-Ir(ppy)$_2$(ppz), we carried out a kinetic analysis for fs-XTA spectra and time profiles using the following three candidate reaction schemes:

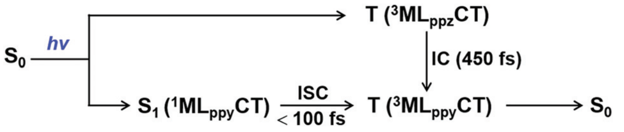

(1)

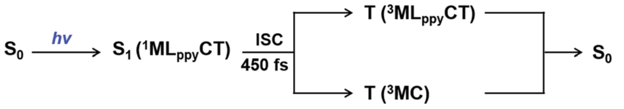

(2)

$$S_0 \xrightarrow{hv} S_1(^1\mathrm{ML_{ppy}CT}) \underset{<100\,\mathrm{fs}}{\xrightarrow{\mathrm{ISC}}} T(^3\mathrm{ML_{ppy}CT}) \xrightarrow{450\,\mathrm{fs}} T(^3\mathrm{MC}) \rightarrow S_0 \quad (3)$$

For each kinetic model, the experimental curves and time profiles were compared with the simulated curves using the obtained time constant (450 fs). As shown in Fig. 6, reaction (1) gives the best fit for the experimental curves and time profiles. Reactions (2) and (3) cannot reproduce the experimental data. When the XTA spectra and time profiles were compared with the simulated ones for reaction (2), the best fit was obtained with the ^{3}ML$_{ppy}$CT : ^{3}MC ratio of 75 : 25. However, this best fit with reaction (2) could not describe the experimental difference curves at the negative peak of 11.218 keV and the positive peak of 11.221 keV. Reaction (3) gives the worst agreement for the time profiles, indicating that the direct ^{3}MLCT → ^{3}MC transition does not occur. These results with three candidate reaction schemes support that the fast dynamics of ∼450 fs observed from both XTA and TA experiments corresponds to the IC process from ^{3}ML$_{ppz}$CT to ^{3}ML$_{ppy}$CT. The proposed excited state relaxation dynamics for *fac*-Ir(ppy)$_2$(ppz) in acetonitrile is shown in Fig. 7. The excitation at 400 nm can induce the ^{3}ML$_{ppz}$CT ← S$_0$ transition as well as the ^{1}ML$_{ppy}$CT ← S$_0$ transition, resulting in the formation of ^{1}ML$_{ppy}$CT as a major component and ^{3}ML$_{ppz}$CT as a minor component. ^{1}ML$_{ppy}$CT relaxes rapidly to ^{3}ML$_{ppy}$CT

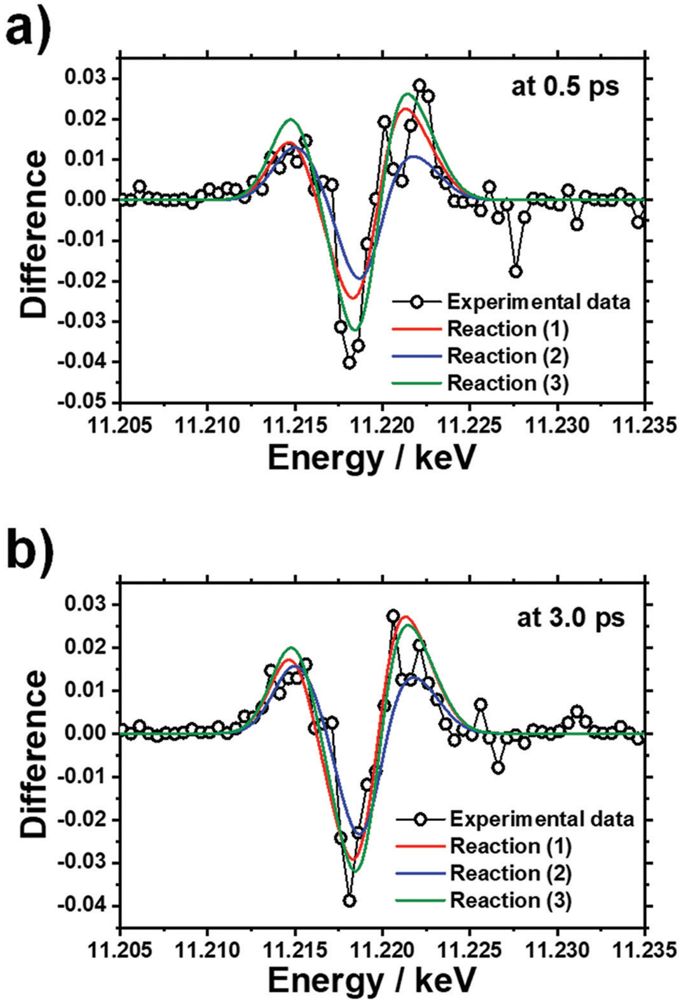

Fig. 6 Fitting of the fs-XTA spectra and time profiles for three candidate reaction schemes. (a and b) XTA spectra obtained at 0.5 and 3.0 ps, respectively. (c) Time profiles monitored at 11.213 (top), 11.218 (middle), and 11.221 keV (bottom).

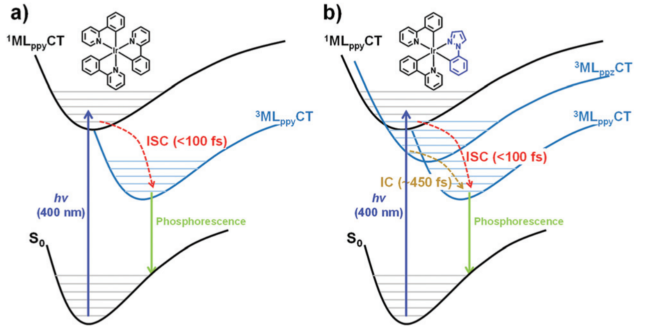

Fig. 7 Energy diagrams for the ultrafast excited state relaxation dynamics of (a) *fac*-Ir(ppy)$_3$ and (b) *fac*-Ir(ppy)$_2$(ppz) in acetonitrile.

through the ISC process within 100 fs. The population on $^3ML_{ppz}CT$ relaxes to $^3ML_{ppy}CT$ through the IC process with a time constant of 450 fs. The fraction of the ultrafast component (~450 fs) determined from the fs-TA experiment was determined to be about 10% from the change in the amplitude of the time profile recorded at the long wavelength (Fig. 4b). This means that 10% of the excited molecules relax to the $^3ML_{ppy}CT$ state through the $^3ML_{ppz}CT$ state, while 90% of the excited molecules relax from the $^1ML_{ppy}CT$ state to the $^3ML_{ppy}CT$ state through ISC. The absence of LLCT or LLET in *fac*-Ir(ppy)$_2$(ppz) is probably due to the large nonadiabatic coupling as well as the small energy gap between $^3ML_{ppz}CT$ and $^3ML_{ppy}CT$ states, resulting in fast IC from $^3ML_{ppz}CT$ to $^3ML_{ppy}CT$.

Conclusions

Applying Ir(III) complexes to OLEDs and artificial photosynthesis systems demands an accurate understanding of their photophysical properties. In this respect, numerous experimental and theoretical approaches for various Ir(III) complexes have been conducted, but the fast excited state relaxation dynamics of Ir(III) complexes with homoleptic or heteroleptic ligand systems is still elusive. Systematic studies for a heteroleptic Ir(III) complex, which shows more complicated photophysical dynamics compared to a homoleptic Ir(III) complex, have been demanded. To address this issue, we investigated the fast excited state relaxation dynamics of *fac*-Ir(ppy)$_2$(ppz) in acetonitrile using the combined time-resolved spectroscopic techniques of fs-XTA and TA and DFT and TDDFT calculations. The experimental and calculation results demonstrate that the $^3ML_{ppz}CT$ state generated by the spin-forbidden transition rapidly relaxes to $^3ML_{ppy}CT$ through the IC process with a time constant of ~450 fs. Such a fast IC from $^3ML_{ppz}CT$ to $^3ML_{ppy}CT$ experimentally measured using fs-XTA and TA is the first instance observed for Ir(III) complexes despite numerous studies. The formation of $^3ML_{ppy}CT$, the lowest ^3MLCT, induces a conformational change of *fac*-Ir(ppy)$_2$(ppz) involving a change in Ir–C or Ir–N bond lengths. The fast IC for *fac*-Ir(ppy)$_2$(ppz) is due to the large nonadiabatic coupling as well as the small energy gap between $^3ML_{ppz}CT$ and $^3ML_{ppy}CT$ states. The results demonstrate that the degree of nonadiabatic coupling between the coupled states and the energy gap between cyclometallating and ancillary ligands play an important role in the excited state relaxation dynamics. Our study should aid in understanding the excited state relaxation dynamics of cyclometalated Ir(III) complexes.

Author contributions

J.C., K.-R.W., and H.I. designed the research; J.C., M.A., J.H.L., D.-S.A., H.K., I.O., C.W.A., E.H.C., Y.L., S.L., J.K., D.W.C., K.-R.W., and H.I. performed the research; J.C., J.H.L., D.-S.A., H.K., I.O., C.W.A., E.H.C., Y.L., S.L., J.K., D.W.C., K.-R.W., and H.I. contributed to the interpretation of the results and J.C., K.-R.W., and H.I. wrote the paper.

Conflicts of interest

There are no conflicts to declare.

Acknowledgements

We thank Sae Hwan Chun, Sunam Kim, Intae Eom, and Minseok Kim for their experimental assistance. This work was supported by the Basic Science Research Program through the National Research Foundation of Korea (NRF), funded by the Ministry of Education (NRF-2017R1C1B1010736, NRF-2020R1C1C1009007 and NRF-2020R1I1A3054352). The fs-XTA experiments were performed at beamline XSS of PAL-XFEL (proposal no. 2018-2nd-XSS-012). This work was supported by the Institute for Basic Science (IBS-R004).

Notes and references

1 Y. You and S. Y. Park, Phosphorescent Iridium(III) Complexes: toward High Phosphorescence Quantum Efficiency through Ligand Control, *Dalton Trans.*, 2009, 1267–1282.

2 K. Hasan, A. K. Bansal, I. D. W. Samuel, C. Roldan-Carmona, H. J. Bolink and E. Zysman-Colman, Tuning the Emission of Cationic Iridium(III) Complexes Towards the Red Through Methoxy Substitution of the Cyclometalating Ligand, *Sci. Rep.*, 2015, **5**, 12325.

3 A. R. Yusoff, A. J. Huckaba and M. K. Nazeeruddin, Phosphorescent Neutral Iridium(III) Complexes for Organic Light-Emitting Diodes, *Top. Curr. Chem.*, 2017, **375**, 39.

4 M. L. P. Reddy and K. S. Bejoymohandas, Evolution of 2, 3′-Bipyridine Class of Cyclometalating Ligands as Efficient Phosphorescent Iridium(III) Emitters for Applications in Organic Light Emitting Diodes, *J. Photochem. Photobiol., C*, 2016, **29**, 29–47.

5 R. Ragni, V. Maiorano, M. Pugliese, A. Maggiore, E. Orselli, F. Babudri, G. Gigli, L. De Cola and G. M. Farinola, A Highly Fluorinated Iridium Complex as a Blue-green Emitting Component for White Electroluminescence, *Synth. Met.*, 2017, **227**, 148–155.

6 T.-H. Kwon, H. S. Cho, M. K. Kim, J.-W. Kim, J.-J. Kim, K. H. Lee, S. J. Park, I.-S. Shin, H. Kim, D. M. Shin, Y. K. Chung and J.-I. Hong, Color Tuning of Cyclometalated Iridium Complexes through Modification of Phenylpyrazole Derivatives and Ancillary Ligand Based on ab Initio Calculations, *Organometallics*, 2005, **24**, 1578–1585.

7 Z. Yan, Y. Wang, J. Ding, Y. Wang and L. Wang, Highly Efficient Phosphorescent Furo[3,2-c]pyridine Based Iridium Complexes with Tunable Emission Colors over the Whole Visible Range, *ACS Appl. Mater. Interfaces*, 2018, **10**, 1888–1896.

8 O. S. Wenger, Proton-coupled Electron Transfer with Photoexcited Ruthenium(II), Rhenium(I), and Iridium(III) Complexes, *Coord. Chem. Rev.*, 2015, **282**, 150–158.

9 A. A. Cordones, J. H. Lee, K. Hong, H. Cho, K. Garg, M. Boggio-Pasqua, J. J. Rack, N. Huse, R. W. Schoenlein and T. K. Kim, Transient Metal-centered States Mediate Isomerization of a Photochromic Ruthenium-sulfoxide Complex, *Nat. Commun.*, 2018, **9**, 1989.

10 G. Alcover-Fortuny, J. F. Wu, R. Caballol and C. de Graaf, Quantum Chemical Study of the Interligand Electron Transfer in Ru Polypyridyl Complexes, *J. Phys. Chem. A*, 2018, **122**, 1114–1123.

11 B. P. Rimgard, J. Fohlinger, J. Petersson, M. Lundberg, B. Zietz, A. M. Woys, S. A. Miller, M. R. Wasielewski and L. Hammarstrom, Ultrafast Interligand Electron Transfer in Cis-$[\mathrm{Ru(4,4'\text{-}dicarboxylate\text{-}2,2'\text{-}bipyridine)_2(NCS)_2}]^{4-}$ and Implications for Electron Injection Limitations in Dye Sensitized Solar Cells, *Chem. Sci.*, 2018, **9**, 7958–7967.

12 R. Ghosh and D. K. Palit, Probing Excited State Charge Transfer Dynamics in a Heteroleptic Ruthenium Complex, *Phys. Chem. Chem. Phys.*, 2014, **16**, 219–226.

13 S. Sato, Y. Matubara, K. Koike, M. Falkenstrom, T. Katayama, Y. Ishibashi, H. Miyasaka, S. Taniguchi, H. Chosrowjan, N. Mataga, N. Fukazawa, S. Koshihara, K. Onda and O. Ishitani, Photochemistry of *fac*-[Re(bpy)$(CO)_3$Cl], *Chem. – Eur. J.*, 2012, **18**, 15722–15734.

14 H. Y. V. Ching, X. Wang, M. He, N. Perujo Holland, R. Guillot, C. Slim, S. Griveau, H. C. Bertrand, C. Policar, F. Bedioui and M. Fontecave, Rhenium Complexes Based on 2-Pyridyl-1,2,3-triazole Ligands: A New Class of CO_2 Reduction Catalysts, *Inorg. Chem.*, 2017, **56**, 2966–2976.

15 C. Hille and F. E. Kühn, Cationic Rhenium Complexes Ligated with N-Heterocyclic Carbenes – an Overview, *Dalton Trans.*, 2016, **45**, 15–31.

16 H. Yang, G. Y. Meng, Y. Y. Zhou, H. J. Tang, J. S. Zhao and Z. L. Wang, The Photoluminescent Properties of New Cationic Iridium(III) Complexes Using Different Anions and Their Applications in White Light-Emitting Diodes, *Materials*, 2015, **8**, 6105–6116.

17 A. B. Tamayo, S. Garon, T. Sajoto, P. I. Djurovich, I. M. Tsyba, R. Bau and M. E. Thompson, Cationic Bis-Cyclometalated Iridium(III) Diimine Complexes and Their Use in Efficient Blue, Green, and Red Electroluminescent Devices, *Inorg. Chem.*, 2005, **44**, 8723–8732.

18 M. Chen, S. Wang, X. Song and L. He, Elucidating the Nonradiative Deactivation Pathways in a Cationic Iridium Complex with 2,4-di(1H-pyrazol-1-yl)Pyridine as the Ancillary Ligand, *J. Phys. Chem. C*, 2018, **122**, 28256–28264.

19 X.-Y. Liu, Y.-H. Zhang, W.-H. Fang and G. Cui, Early-Time Excited-State Relaxation Dynamics of Iridium Compounds: Distinct Roles of Electron and Hole Transfer, *J. Phys. Chem. A*, 2018, **122**, 5518–5532.

20 Y. Kuramochi and O. Ishitani, An Ir(III) Complex Photosensitizer With Strong Visible Light Absorption for Photocatalytic CO_2 Reduction, *Front. Chem.*, 2019, **7**, 259.

21 S. Lee, Y. You, K. Ohkubo, S. Fukuzumi and W. Nam, Highly Efficient Cycloreversion of Photochromic Dithienylethene Compounds Using Visible Light-driven Photoredox Catalysis, *Chem. Sci.*, 2014, **5**, 1463–1474.

22 I. N. Mills, J. A. Porras and S. Bernhard, Judicious Design of Cationic, Cyclometalated Ir(III) Complexes for Photochemical Energy Conversion and Optoelectronics, *Acc. Chem. Res.*, 2018, **51**, 352–364.

23 C.-O. Ng, H. Feng, S.-C. Cheng, Y. Xiao, L. T.-L. Lo and C.-C. Ko, Photoredox Catalysis of Cyclometalated IrIII Complex for the Conversion of Amines to Fluorinated Alkyl Amides, *Asian J. Org. Chem.*, 2018, **7**, 1587–1590.

24 S. Sato, T. Morikawa, T. Kajino and O. Ishitani, A Highly Efficient Mononuclear Iridium Complex Photocatalyst for CO_2 Reduction under Visible Light, *Angew. Chem., Int. Ed.*, 2013, **52**, 988–992.

25 H. Tian, H. Shimakoshi, G. Park, S. Kim, Y. You and Y. Hisaeda, Photocatalytic Function of the B12 Complex with the Cyclometalated Iridium(III) Complex as a Photosensitizer under Visible Light Irradiation, *Dalton Trans.*, 2018, **47**, 675–683.

26 S. Tschierlei, A. Neubauer, N. Rockstroh, M. Karnahl, P. Schwarzbach, H. Junge, M. Beller and S. Lochbrunner, Ultrafast Excited State Dynamics of Iridium(III) Complexes and Their Changes upon Immobilisation onto Titanium Dioxide Layers, *Phys. Chem. Chem. Phys.*, 2016, **18**, 10682–10687.

27 Y. You, K. S. Kim, T. K. Ahn, D. Kim and S. Y. Park, Direct Spectroscopic Observation of Interligand Energy Transfer in Cyclometalated Heteroleptic Iridium(III) Complexes: A Strategy for Phosphorescence Color Tuning and White Light Generation, *J. Phys. Chem. C*, 2007, **111**, 4052–4060.

28 Y. You, J. Seo, S. H. Kim, K. S. Kim, T. K. Ahn, D. Kim and S. Y. Park, Highly Phosphorescent Iridium Complexes with Chromophoric 2-(2-Hydroxyphenyl)oxazole-Based Ancillary Ligands: Interligand Energy-Harvesting Phosphorescence, *Inorg. Chem.*, 2008, **47**, 1476–1487.

29 M. S. Mehata, Y. Yang, Z. J. Qu, J. S. Chen, F. J. Zhao and K. L. Han, Spin Mixed Charge Transfer States of Iridium

Complex Ir(ppy)$_3$: Transient Absorption and Time-resolved Photoluminescence, *RSC Adv.*, 2015, **5**, 34094–34099.

30 G. J. Hedley, A. Ruseckas and I. D. W. Samuel, Ultrafast Intersystem Crossing in a Red Phosphorescent Iridium Complex, *J. Phys. Chem. A*, 2009, **113**, 2–4.

31 Y.-J. Cho, S.-Y. Kim, M. Cho, K.-R. Wee, H.-J. Son, W.-S. Han, D. W. Cho and S. O. Kang, Ligand-to-ligand Charge Transfer in Heteroleptic Ir-complexes: Comprehensive Investigations of Its Fast Dynamics and Mechanism, *Phys. Chem. Chem. Phys.*, 2016, **18**, 15162–15169.

32 E. Pomarico, M. Silatani, F. Messina, O. Braem, A. Cannizzo, E. Barranoff, J. H. Klein, C. Lambert and M. Chergui, Dual Luminescence, Interligand Decay, and Nonradiative Electronic Relaxation of Cyclometalated Iridium Complexes in Solution, *J. Phys. Chem. C*, 2016, **120**, 16459–16469.

33 T. Sajoto, P. I. Djurovich, A. B. Tamayo, J. Oxgaard, W. A. Goddard and M. E. Thompson, Temperature Dependence of Blue Phosphorescent Cyclometalated Ir(III) Complexes, *J. Am. Chem. Soc.*, 2009, **131**, 9813–9822.

34 S. Arroliga-Rocha and D. Escudero, Facial and Meridional Isomers of Tris(bidentate) Ir(III) Complexes: Unravelling Their Different Excited State Reactivity, *Inorg. Chem.*, 2018, **57**, 12106–12112.

35 M. Kleinschmidt, C. v. Wüllen and C. M. Marian, Intersystem-Crossing and Phosphorescence Rates in *fac*-Ir^{III}(ppy)$_3$: A Theoretical Study Involving Multi-reference Configuration Interaction Wavefunctions, *J. Chem. Phys.*, 2015, **142**, 094301.

36 K. A. King and R. J. Watts, Dual Emission from an *ortho*-Metalated Iridium(III) Complex, *J. Am. Chem. Soc.*, 1987, **109**, 1589–1590.

37 G. J. Hedley, A. Ruseckas and I. D. W. Samuel, Vibrational Energy Flow Controls Internal Conversion in a Transition Metal Complex, *J. Phys. Chem. A*, 2010, **114**, 8961–8968.

38 Y.-J. Cho, S.-Y. Kim, H.-J. Son, W.-S. Han, D. W. Cho and S. O. Kang, Comprehensive Spectroscopic Studies of *cis* and trans Isomers of Red-phosphorescent Heteroleptic Iridium(III) Complexes, *J. Photochem. Photobiol., A*, 2018, **356**, 673–680.

39 A. J. Howarth, D. L. Davies, F. Lelj, M. O. Wolf and B. O. Patrick, Tuning the Emission Lifetime in Bis-cyclometalated Iridium(III) Complexes Bearing Iminopyrene Ligands, *Inorg. Chem.*, 2014, **53**, 11882–11889.

40 R. Lincoln, L. Kohler, S. Monro, H. Yin, M. Stephenson, R. Zong, A. Chouai, C. Dorsey, R. Hennigar, R. P. Thummel and S. A. McFarland, Exploitation of Long-Lived ^{3}IL Excited States for Metal–Organic Photodynamic Therapy: Verification in a Metastatic Melanoma Model, *J. Am. Chem. Soc.*, 2013, **135**, 17161–17175.

41 Z. Li, P. Cui, C. Wang, S. Kilina and W. Sun, Nonlinear Absorbing Cationic Bipyridyl Iridium(III) Complexes Bearing Cyclometalating Ligands with Different Degrees of π-Conjugation: Synthesis, Photophysics, and Reverse Saturable Absorption, *J. Phys. Chem. C*, 2014, **118**, 28764–28775.

42 C. L. Ho and W. Y. Wong, Charge and Energy Transfers in Functional Metallophosphors and Metallopolyynes, *Coord. Chem. Rev.*, 2013, **257**, 1614–1649.

43 S.-H. Wu, J.-W. Ling, S.-H. Lai, M.-J. Huang, C. H. Cheng and I. C. Chen, Dynamics of the Excited States of [Ir(ppy)$_2$bpy]$^+$ with Triple Phosphorescence, *J. Phys. Chem. A*, 2010, **114**, 10339–10344.

44 R. Bevernaegie, L. Marcelis, A. Moreno-Betancourt, B. Laramee-Milette, G. S. Hanan, F. Loiseau, M. Sliwa and B. Elias, Ultrafast Charge Transfer Excited State Dynamics in Trifluoromethyl-substituted Iridium(III) Complexes, *Phys. Chem. Chem. Phys.*, 2018, **20**, 27256–27260.

45 Y.-J. Cho, S.-Y. Kim, H.-J. Son, D. W. Cho and S. O. Kang, The Effect of Interligand Energy Transfer on the Emission Spectra of Heteroleptic Ir Complexes, *Phys. Chem. Chem. Phys.*, 2017, **19**, 8778–8786.

46 P. A. Scattergood, A. M. Ranieri, L. Charalambou, A. Comia, D. A. W. Ross, C. R. Rice, S. J. O. Hardman, J.-L. Heully, I. M. Dixon, M. Massi, F. Alary and P. I. P. Elliott, Unravelling the Mechanism of Excited-State Interligand Energy Transfer and the Engineering of Dual Emission in [Ir(C^N)$_2$(N^N)]$^+$ Complexes, *Inorg. Chem.*, 2020, **59**, 1785–1803.

47 J. P. F. Nunes, K. Ledbetter, M. Lin, M. Kozina, D. P. DePonte, E. Biasin, M. Centurion, C. J. Crissman, M. Dunning, S. Guillet, K. Jobe, Y. Liu, M. Mo, X. Shen, R. Sublett, S. Weathersby, C. Yoneda, T. J. A. Wolf, J. Yang, A. A. Cordones and X. J. Wang, Liquid-phase Mega-electron-volt Ultrafast Electron Diffraction, *Struct. Dyn.*, 2020, **7**, 024301.

48 K. J. Mohler, D. Ehberger, I. Gronwald, C. Lange, R. Huber and P. Baum, Ultrafast Electron Diffraction from Nanophotonic Waveforms via Dynamical Aharonov-Bohm Phases, *Sci. Adv.*, 2020, **6**, eabc8804.

49 Y. Jiang, L. C. Liu, H. M. Müller-Werkmeister, C. Lu, D. Zhang, R. L. Field, A. Sarracini, G. Moriena, E. Collet and R. J. D. Miller, Structural Dynamics upon Photoexcitation in a Spin Crossover Crystal Probed with Femtosecond Electron Diffraction, *Angew. Chem., Int. Ed.*, 2017, **56**, 7130–7134.

50 J. Cao, Z. Hao, H. Park, C. Tao, D. Kau and L. Blaszczyk, Femtosecond Electron Diffraction for Direct Measurement of Ultrafast Atomic Motions, *Appl. Phys. Lett.*, 2003, **83**, 1044–1046.

51 J. Yang, X. Zhu, J. P. F. Nunes, J. K. Yu, R. M. Parrish, T. J. A. Wolf, M. Centurion, M. Gühr, R. Li, Y. Liu, B. Moore, M. Niebuhr, S. Park, X. Shen, S. Weathersby, T. Weinacht, T. J. Martinez and X. Wang, Simultaneous Observation of Nuclear and Electronic Dynamics by Ultrafast Electron Diffraction, *Science*, 2020, **368**, 885–889.

52 H. Ihee, M. Lorenc, T. K. Kim, Q. Y. Kong, M. Cammarata, J. H. Lee, S. Bratos and M. Wulff, Ultrafast X-ray Diffraction of Transient Molecular Structures in Solution, *Science*, 2005, **309**, 1223–1227.

53 M. Christensen, K. Haldrup, K. Bechgaard, R. Feidenhans'l, Q. Kong, M. Cammarata, M. L. Russo, M. Wulff, N. Harrit and M. M. Nielsen, Time-Resolved X-ray Scattering of an Electronically Excited State in Solution. Structure of the $^3A_{2u}$ State of Tetrakis-μ-pyrophosphitodiplatinate(II), *J. Am. Chem. Soc.*, 2009, **131**, 502–508.

54 E. Biasin, T. B. van Driel, G. Levi, M. G. Laursen, A. O. Dohn, A. Moltke, P. Vester, F. B. K. Hansen, K. S. Kjaer, T. Harlang, R. Hartsock, M. Christensen, K. J. Gaffney, N. E. Henriksen, K. B. Møller, K. Haldrup and M. M. Nielsen, Anisotropy Enhanced X-ray Scattering from Solvated Transition Metal Complexes, *J. Synchrotron Radiat.*, 2018, **25**, 306–315.

55 J. G. Kim, S. Nozawa, H. Kim, E. H. Choi, T. Sato, T. W. Kim, K. H. Kim, H. Ki, J. Kim, M. Choi, Y. Lee, J. Heo, K. Y. Oang, K. Ichiyanagi, R. Fukaya, J. H. Lee, J. Park, I. Eom, S. H. Chun, S. Kim, M. Kim, T. Katayama, T. Togashi, S. Owada, M. Yabashi, S. J. Lee, S. Lee, C. W. Ahn, D.-S. Ahn, J. Moon, S. Choi, J. Kim, T. Joo, J. Kim, S.-i. Adachi and H. Ihee, Mapping the Emergence of Molecular Vibrations Mediating Bond Formation, *Nature*, 2020, **582**, 520–524.

56 K. H. Kim, J. G. Kim, S. Nozawa, T. Sato, K. Y. Oang, T. W. Kim, H. Ki, J. Jo, S. Park, C. Song, T. Sato, K. Ogawa, T. Togashi, K. Tono, M. Yabashi, T. Ishikawa, J. Kim, R. Ryoo, J. Kim, H. Ihee and S.-i. Adachi, Direct Observation of Bond Formation in Solution with Femtosecond X-ray Scattering, *Nature*, 2015, **518**, 385–389.

57 D. J. Hsu, D. Leshchev, D. Rimmerman, J. Hong, M. S. Kelley, I. Kosheleva, X. Zhang and L. X. Chen, X-ray Snapshots Reveal Conformational Influence on Active Site Ligation during Metalloprotein Folding, *Chem. Sci.*, 2019, **10**, 9788–9800.

58 E. Claesson, W. Y. Wahlgren, H. Takala, S. Pandey, L. Castillon, V. Kuznetsova, L. Henry, M. Panman, M. Carrillo, J. Kübel, R. Nanekar, L. Isaksson, A. Nimmrich, A. Cellini, D. Morozov, M. Maj, M. Kurttila, R. Bosman, E. Nango, R. Tanaka, T. Tanaka, L. Fangjia, S. Iwata, S. Owada, K. Moffat, G. Groenhof, E. A. Stojković, J. A. Ihalainen, M. Schmidt and S. Westenhoff, The Primary Structural Photoresponse of Phytochrome Proteins Captured by a Femtosecond X-ray Laser, *eLife*, 2020, **9**, e53514.

59 G. Brändén, G. Hammarin, R. Harimoorthy, A. Johansson, D. Arnlund, E. Malmerberg, A. Barty, S. Tångefjord, P. Berntsen, D. P. DePonte, C. Seuring, T. A. White, F. Stellato, R. Bean, K. R. Beyerlein, L. M. G. Chavas, H. Fleckenstein, C. Gati, U. Ghoshdastider, L. Gumprecht, D. Oberthür, D. Popp, M. Seibert, T. Tilp, M. Messerschmidt, G. J. Williams, N. D. Loh, H. N. Chapman, P. Zwart, M. Liang, S. Boutet, R. C. Robinson and R. Neutze, Coherent Diffractive Imaging of Microtubules Using an X-ray Laser, *Nat. Commun.*, 2019, **10**, 2589.

60 H. Ihee, Visualizing Solution-Phase Reaction Dynamics with Time-Resolved X-ray Liquidography, *Acc. Chem. Res.*, 2009, **42**, 356–366.

61 A. Britz, B. Abraham, E. Biasin, T. B. van Driel, A. Gallo, A. T. Garcia-Esparza, J. Glownia, A. Loukianov, S. Nelson, M. Reinhard, D. Sokaras and R. Alonso-Mori, Resolving Structures of Transition Metal Complex Reaction Intermediates with Femtosecond EXAFS, *Phys. Chem. Chem. Phys.*, 2020, **22**, 2660–2666.

62 J. Kim, K. H. Kim, K. Y. Oang, J. H. Lee, K. Hong, H. Cho, N. Huse, R. W. Schoenlein, T. K. Kim and H. Ihee, Tracking Reaction Dynamics in Solution by Pump–Probe X-ray Absorption Spectroscopy and X-ray Liquidography (Solution Scattering), *Chem. Commun.*, 2016, **52**, 3734–3749.

63 M. Fondell, S. Eckert, R. M. Jay, C. Weniger, W. Quevedo, J. Niskanen, B. Kennedy, F. Sorgenfrei, D. Schick, E. Giangrisostomi, R. Ovsyannikov, K. Adamczyk, N. Huse, P. Wernet, R. Mitzner and A. Föhlisch, Time-resolved Soft X-ray Absorption Spectroscopy in Transmission Mode on Liquids at MHz Repetition Rates, *Struct. Dyn.*, 2017, **4**, 054902.

64 T. Katayama, T. Northey, W. Gawelda, C. J. Milne, G. Vankó, F. A. Lima, R. Bohinc, Z. Németh, S. Nozawa, T. Sato, D. Khakhulin, J. Szlachetko, T. Togashi, S. Owada, S.-i. Adachi, C. Bressler, M. Yabashi and T. J. Penfold, Tracking Multiple Components of a Nuclear Wavepacket in Photoexcited Cu(I)-phenanthroline Complex Using Ultrafast X-ray Spectroscopy, *Nat. Commun.*, 2019, **10**, 3606.

65 M. L. Shelby, P. J. Lestrange, N. E. Jackson, K. Haldrup, M. W. Mara, A. B. Stickrath, D. Zhu, H. T. Lemke, M. Chollet, B. M. Hoffman, X. Li and L. X. Chen, Ultrafast Excited State Relaxation of a Metalloporphyrin Revealed by Femtosecond X-ray Absorption Spectroscopy, *J. Am. Chem. Soc.*, 2016, **138**, 8752–8764.

66 A. O. Er, J. Chen and P. M. Rentzepis, Ultrafast Time Resolved X-ray Diffraction, Extended X-ray Absorption Fine Structure and X-ray Absorption Near Edge Structure, *J. Appl. Phys.*, 2012, **112**, 031101.

67 W. Zhang, K. S. Kjær, R. Alonso-Mori, U. Bergmann, M. Chollet, L. A. Fredin, R. G. Hadt, R. W. Hartsock, T. Harlang, T. Kroll, K. Kubiček, H. T. Lemke, H. W. Liang, Y. Liu, M. M. Nielsen, P. Persson, J. S. Robinson, E. I. Solomon, Z. Sun, D. Sokaras, T. B. van Driel, T.-C. Weng, D. Zhu, K. Wärnmark, V. Sundström and K. J. Gaffney, Manipulating Charge Transfer Excited State Relaxation and Spin Crossover in Iron Coordination Complexes with Ligand Substitution, *Chem. Sci.*, 2017, **8**, 515–523.

68 S. Reich, J. Göttlicher, A. Ziefuss, R. Streubel, A. Letzel, A. Menzel, O. Mathon, S. Pascarelli, T. Baumbach, M. Zuber, B. Gökce, S. Barcikowski and A. Plech, In Situ Speciation and Spatial Mapping of Zn Products during Pulsed Laser Ablation in Liquids (PLAL) by Combined Synchrotron Methods, *Nanoscale*, 2020, **12**, 14011–14020.

69 S. A. Denisov, Y. Cudre, P. Verwilst, G. Jonusauskas, M. Marin-Suarez, J. F. Fernandez-Sanchez, E. Baranoff and N. D. McClenaghan, Direct Observation of Reversible Electronic Energy Transfer Involving an Iridium Center, *Inorg. Chem.*, 2014, **53**, 2677–2682.

70 K. Shimomura, H. Kai, Y. Nakamura, Y. Hong, S. Mori, K. Miki, K. Ohe, Y. Notsuka, Y. Yamaoka, M. Ishida, D. Kim and H. Furuta, Bis-Metal Complexes of Doubly N-Confused Dioxohexaphyrins as Potential Near-Infrared-II Photoacoustic Dyes, *J. Am. Chem. Soc.*, 2020, **142**, 4429–4437.

71 D. Göries, B. Dicke, P. Roedig, N. Stübe, J. Meyer, A. Galler, W. Gawelda, A. Britz, P. Geßler, H. S. Namin, A. Beckmann, M. Schlie, M. Warmer, M. Naumova, C. Bressler, M. Rübhausen, E. Weckert and A. Meents, Time-resolved Pump and Probe X-ray Absorption Fine Structure Spectroscopy at Beamline P11 at PETRA III, *Rev. Sci. Instrum.*, 2016, **87**, 053116.

72 A. Britz, Ph. D, Dissertation, University Hamburg, 2016.

73 M. Silatani, Ph. D, Dissertation, EPFL n° 6797, 2015.

74 G. C. O'Neil, L. Miaja-Avila, Y. I. Joe, B. K. Alpert, M. Balasubramanian, D. M. Sagar, W. Doriese, J. W. Fowler, W. K. Fullagar, N. Chen, G. C. Hilton, R. Jimenez, B. Ravel, C. D. Reintsema, D. R. Schmidt, K. L. Silverman, D. S. Swetz, J. Uhlig and J. N. Ullom, Ultrafast Time-Resolved X-ray Absorption Spectroscopy of Ferrioxalate Photolysis with a Laser Plasma X-ray Source and Microcalorimeter Array, *J. Phys. Chem. Lett.*, 2017, **8**, 1099–1104.

75 W. Gawelda, M. Johnson, F. M. F. de Groot, R. Abela, C. Bressler and M. Chergui, Electronic and Molecular Structure of Photoexcited $[\mathrm{Ru^{II}(bpy)_3}]^{2+}$ Probed by Picosecond X-ray Absorption Spectroscopy, *J. Am. Chem. Soc.*, 2006, **128**, 5001–5009.

76 H. Wang, Q. Liao, H. Fu, Y. Zeng, Z. Jiang, J. Ma and J. Yao, $\mathrm{Ir(ppy)_3}$ Phosphorescent Microrods and Nanowires: Promising Micro-Phosphors, *J. Mater. Chem.*, 2009, **19**, 89–96.

77 T. Hofbeck and H. Yersin, The Triplet State of fac-$\mathrm{Ir(ppy)_3}$, *Inorg. Chem.*, 2010, **49**, 9290–9299.

78 M. E. Mohanty, C. Madhu, V. L. Reddy, M. Paramasivam, P. R. Bangal and V. J. Rao, Direct Observation of the Rise of Delayed Fluorescence in Dithienylbenzothiadiazole and Its Role in the Excited State Dynamics of a Donor–Acceptor–Donor Molecule, *Phys. Chem. Chem. Phys.*, 2017, **19**, 9118–9127.

79 S. K. Rajagopal, A. R. Mallia and M. Hariharan, Enhanced Intersystem Crossing in Carbonylpyrenes, *Phys. Chem. Chem. Phys.*, 2017, **19**, 28225–28231.